



Targeting LIMK1 in Alzheimer's Disease: A Multifaceted Computational Investigation Involving ADMET, Virtual Screening, Molecular Docking, and Molecular Dynamics

Defne Eşkin¹ , Harun Nalçakan¹ , Gülbin Kurtay^{2*} , Yiğit Akkan² , Mazlum Türk² ,
Beril Uras² 

¹Ankara University, Department of Chemistry, Ankara, 06100, Turkey.

²Hacettepe University, Department of Chemistry, Ankara, 06800, Turkey.

Abstract: LIM domain kinases (LIMKs), which include LIMK1 and LIMK2, are key proteins in actin dynamics. On this basis, the inhibition of LIMK1 enhances dendritic spine density and size in dementia, reducing Alzheimer's disease (AD) effects. Therefore, several small molecules were discovered as potential therapeutic targets for AD. Herein, a pharmacophore-based virtual screening was employed to identify novel potential LIMK1 inhibitors. The pharmacophore model derived from the co-crystallized receptor structure of PubChem-329823760: LIMK1 (PDB ID: 5NXC) was then used for virtual screening. After applying Lipinski's rules and pharmacophore filters, 29 potential hits were identified. Molecular docking simulations were performed to determine the binding affinities of these candidates against LIMK1, with results ranging from -5.20 to -10.60 kcal/mol. Notably, PubChem-136621040 showed the highest binding affinity against the target protein, with a docking score of -10.60 kcal/mol, slightly surpassing the native ligand, PubChem-329823760, possessing a lower docking score of -9.80 kcal/mol. The drug-likeness and toxicity properties of target compounds were assessed through ADMET evaluations. A series of 75 nanosecond molecular dynamics (MD) simulations were conducted on the complexes generated by the best-docked molecule and the native ligand. RMSD, RMSF, SASA, and Rg calculations of their trajectories were also calculated. PubChem-136621040 possessed an average RMSD value of 0.23 nm, lower than the native ligand's 0.31 nm, indicating a greater binding stability. The RMSF results also revealed that the best-docked compound had a lower value (0.10 nm), while the native ligand possessed a value of 0.12 nm. The SASA values for both the native ligand and the best-docked compound were nearly identical, at 150.20 nm² and 150.80 nm², respectively. The Rg results demonstrated that both complexes maintained their rigidity throughout the simulation, with similar average values of 2.04 nm for the native ligand and 2.06 nm for the best-docked compound.

Keywords: ADMET, LIM kinases, molecular docking, molecular dynamics, virtual screening.

Submitted: April 5, 2024. **Accepted:** September 6, 2024.

Cite this: Eşkin D, Nalçakan H, Kurtay G, Akkan Y, Türk M, Uras B. Targeting LIMK1 in Alzheimer's Disease: A Multifaceted Computational Investigation Involving ADMET, Virtual Screening, Molecular Docking, and Molecular Dynamics. JOTCSA. 2024;11(4): 1425-40.

DOI: <https://doi.org/10.18596/jotcsa.1465547>

***Corresponding author's E-mail:** gulbinkurtay@hacettepe.edu.tr

1. INTRODUCTION

Alzheimer's disease (AD) is a neurodegenerative disorder that progressively decreases cognitive abilities, ultimately resulting in the death of the affected individuals. Recent studies have indicated that AD is the leading cause of dementia among older people (1,2). Remarkably, between 60 and 70% of cases in which the older population has increasing levels of cognitive impairment can be linked to Alzheimer's disease (3).

The emergence of abnormally expanded neuronal processes known as dystrophic neurites is one of the primary features of AD patients (4,5). Tau protein, a key indicator of AD pathology, accumulates in these neurites, and when this protein is hyperphosphorylated, it separates from microtubules and subsequently clumps together to form neurofibrillary tangles (6,7). LIM domain kinase proteins (LIMKs), which are essential regulators of the actin cytoskeleton and cellular motility, contribute to the pathophysiology of AD by causing tau to become hyperphosphorylated, which in turn

causes dystrophic neurites to develop and intensify the neurodegenerative cascade in AD (8–11).

The LIM kinase family is typically composed of two types of proteins, specifically LIM domain kinase 1 (LIMK1) and LIM domain kinase 2 (LIMK2). Despite sharing numerous structural similarities, these two macromolecules exhibit distinct expression and subcellular localization patterns, in addition to functional differences (12,13). LIMK1 protein is composed of 633 amino acids that encompass a

variety of functional domains. These domains include the LIM₁ and LIM₂ domains, the PDZ binding motif, and the serine/proline (Ser/Pro)-rich region (14). In addition, it also includes the kinase domain, which contains the S fragment and the nuclear localization signal (NLS) subdomain. It has also been demonstrated that the regulation of kinase activity is significantly influenced by the LIM and PDZ domains (15). The representation of these domains is depicted in Figure 1.

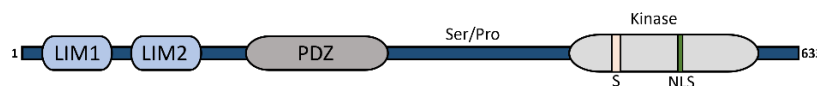


Figure 1: Domain architecture of LIMK1.

These proteins are essential for several physiological functions, including motility, cell cycle control, and brain development. It has been shown that these proteins control the phosphorylation activity of LIMK1 and LIMK2, which influences their capacity to phosphorylate and deactivate cofilin, an essential substrate. It is important to highlight that while LIMK2 is broadly expressed, LIMK1 is primarily present in neural tissues (16). Consequently, among these two proteins, inhibiting LIMK1 could have a more substantial impact on reducing the severity of AD by enhancing the size and density of dendritic spines (17).

In recent years, researchers have focused on the discovery of novel LIMK inhibitors, and various small molecules have been described in the literature. In research, Singh et al. employed similar *in silico* strategies, encompassing pharmacophore-based virtual screening, docking, and ADMET analyses, to identify novel compounds with inhibitory activities against LIMK1 in 2023. They constructed their pharmacophore models and successfully identified three virtual hits based on their compound (18).

In a parallel study, Rangaswamy et al. (2023) pinpointed five potential compounds for LIMK2 inhibition in cancer treatment, which was achieved through pharmacophore-based virtual screening, *in silico* ADMET studies, along with molecular docking and dynamics. Their research highlighted two out of the five compounds as promising candidates that could be further developed for cancer therapy (19).

In 2020, Zhang's group employed an *in silico* virtual screening approach to discover LIMK1 inhibitors for the purpose of inhibiting cell proliferation. Through *in silico* virtual screening, they identified a compound known as luteolin. Subsequent molecular docking assessments and experimental findings of their discovered compound indicated that it has demonstrated significant inhibitory activity against LIMK1 (20).

The literature inquiry offers a comprehensive insight into potential inhibitors of LIMKs and their possible therapeutic applications in various diseases, including neurological disorders and cancer. However, it has been noted that there are only a

limited number of studies specifically investigating the role of LIMK1 activity in Alzheimer's Disease. Therefore, in our study, we initially employed pharmacophore-based virtual screening to detect potential compounds to inhibit LIMK1 for AD treatment. In the subsequent step, the screened candidates were further evaluated with molecular docking simulation along with the determination of ADME (absorption, distribution, metabolism, excretion) profiles using various *in silico* techniques.

The toxicity properties of these screened molecules were also analyzed and calculated to reveal potential risks. Leveraging the findings of these calculations, candidate pharmaceuticals possessing the highest binding affinity and the complex of the native ligand with its macromolecule were further investigated with molecular dynamics simulation {PubChem-329823760: LIMK1 (*native ligand*) and PubChem-136621040: LIMK1 (best-docked ligand) complexes, respectively} to reveal root-mean-square deviation (RMSD), root-mean-square fluctuation (RMSF), solvent-accessible surface area (SASA), and radius of gyration (Rg) graphs to determine the post-dock analysis including binding stability of the system after the docking study, protein rigidity and residue interactions during the MD simulation.

In this scope, our study encompasses the identification and comprehensive analysis of novel LIMK1 inhibitors for the potential treatment of Alzheimer's Disease. Through advanced *in silico* methodologies, including pharmacophore-based virtual screening, molecular docking simulations, and ADME profiling, we aim to evaluate the efficacy, safety, and binding stability of candidate compounds. Furthermore, by employing molecular dynamics simulations, we assess the structural and dynamic behavior of these inhibitors, providing critical insights into their therapeutic potential against LIMK1-mediated neurodegeneration.

In this study, we employed an *in silico* approach to identify candidate molecules with the requisite characteristics for inhibiting the LIMK1 receptor, including the ability to permeate the blood-brain barrier, optimal pharmacokinetic properties, minimal toxicity, and robust binding affinity coupled with binding stability. Our research integrates

methodologies such as pharmacophore-based virtual screening, ADME/T evaluations using various web-based platforms to obtain enhanced pharmacological and pharmacokinetic profiles of the investigated ligands, molecular docking of the compounds to the target receptor, and molecular dynamics (MD) simulations to assess the stability of the docked complexes with LIMK1.

2. COMPUTATIONAL STUDIES

2.1. Pharmacophore-Based Virtual Screening

Pharmacophore-based virtual screening was performed using the Pharmit server (<http://pharmit.csb.pitt.edu>), which allows the use of several databases (PubChem, ZINC, ChEMBL, and Molport, etc.) to identify candidates potentially to inhibit LIMK1. To achieve this, input files of the structure of LIM domain kinase 1 (PDB ID: 5NXC), which is co-crystallized with its native ligand (PubChem-329823) obtained from the RCSB Protein Data Bank (www.rcsb.org), with no mutations in its protein sequence were submitted, and pharmacophore model based on the pharmacophore classes of the native ligand was generated on the server. The initial screening was conducted by applying this pharmacophore model, selecting the PubChem database, which contains a vast collection of 103,302,052 compounds. 419 compounds were discovered through the application of a pharmacophore filter at the initial step. Subsequently, Lipinski's filter was applied to these molecules to identify the desired compounds having the ideal drug-likeness properties. Therefore, parameters to provide the screened ligands to obey this rule were selected. The compounds possessing a molecular weight (MW) lower than 500 Da, hydrogen bond acceptor (HBA) not much than 10, hydrogen bond donor (HBD) less than 5, number of rotatable bonds (nROTb) no more than 10, and $\text{clogP}_{o/w}$ value less than 5 were intentionally configured to eliminate undesired compounds. A total of 78 candidates were successfully obtained following the application of Lipinski's filter. These compounds were further evaluated with the embedded docking application of Pharmit to detect the compounds whose RMSD values are less than 2.0 \AA^2 . As a result, 49 compounds out of 78 hits were also eliminated, and 29 compounds possessing the most desired drug-likeness characteristics were obtained for further analysis.

2.2. Molecular Docking Studies

The docking simulation aimed to generate a comprehensive viewpoint for potential pharmaceuticals that potentially demonstrate their binding ability against LIMK1. For this reason, the OneAngstrom SAMSON platform/2023-R1 software package's AutoDock Vina extension was used to forecast every step of the process, including docking validation, pre-docking preparation, and molecular docking simulations. To verify our chosen docking methodology, docking validation was initially performed, which involved a redocking of the initial conformation of the native ligand with the same structure using our docking parameters. Following this, the native compound was superimposed with

the docked compound, and the RMSD value was computed.

Consequently, pre-docking preparation was concluded for the LIMK1 crystal structure, which was retrieved from the RCSB Protein Data Bank (www.rcsb.org). The macromolecule's co-crystallized native ligand (PubChem-329823) was deleted, along with all ions and water molecules. Subsequently, necessary charges were applied, and hydrogens were included in the system. Since LIMK1 possesses only one chain, no modification, including chain removal, was carried out. Additionally, the target protein and the screened ligands were adjusted to a physiological pH of 7.4. The grid box size was set at $30.00 \times 24.90 \times 24.80 \text{ \AA}^3$ with a grid point spacing of 0.375 \AA , and the center coordinates of the grid box were defined as x: 18.60, y: 16.50, and z: 12.50. The coordinates were also derived using SAMSON, through the identification of the macromolecule's binding site. This operation was performed by selecting an area within a radius of 10.00 \AA around the native ligand.

Furthermore, a library of ligands was constructed from the input file, encompassing 29 potential inhibitors, which was generated in SDF format and downloaded from the Pharmit website. Before the docking procedure, our compounds underwent 5000 steps of energy minimization to determine their most stable conformations. Following the completion of the docking simulation, the top 10 compounds with the highest docking scores were intentionally selected, and their binding affinities, along with the molecular structures, were deeply investigated.

2.3. ADMET Studies

ADME (Absorption, Distribution, Metabolism, and Elimination) evaluations provide valuable insights into a drug's physiological responses and potential interactions. For this reason, evaluating a compound's suitability as a drug candidate requires more than just looking at its docking score; examination of ADME analyses is also necessary. Several web-based platforms, such as SwissADME, PreADMET, OSIRIS, and Molinspiration, were utilized to conduct ADME assessments to evaluate the drug-likeness properties and efficacy of the screened compounds. Furthermore, possible toxicity assessments were assessed using the Syntelly platform, which is based on the application of artificial intelligence to evaluate many toxicity parameters that identify potential negative effects of the pharmaceutical candidates.

2.3.1. SwissADME

SwissADME is a freely available online tool that provides a wide range of information and forecasts about small molecules' physicochemical and pharmacological properties. It also evaluates compounds' ADME, and drug-likeness profiles based on Lipinski's rule of five (RO5), which plays a significant role in drug discovery and development to identify ideal pharmacological properties for candidate small molecules (21). The rule of five outlines essential criteria for assessing the suitability of a compound for drug development. These criteria include a molecular weight (MW) of no more than 500

g/mol, a maximum of 10 hydrogen bond acceptors (HBAs), less than 5 hydrogen bond donors, $\log P_{o/w}$, which indicates the partition coefficient between octanol and water, used to evaluate lipophilicity characteristics not exceeding 5, and topological polar surface area (TPSA) below 140 Å². Moreover, compliance with the rule dictates that the number of rotatable bonds (nROTBs) in a potential pharmaceutical should be less than 9 (22).

2.3.2. PreADMET

ADME properties of our compounds were determined using the PreADMET platform (<http://preadmet.bmdrc.org/>). In this scope, blood-barrier permeability (BBB), passive gastrointestinal absorption (HIA), and protein-plasma binding abilities (PPB) were detected. BBB could be computed as the ratio of steady-state concentrations of radiolabeled compounds in the brain to that in the peripheral blood (23). It is noteworthy that compounds with BBB values less than 0.10 are considered to have low CNS absorption, those with values between 0.10 and 0.20 exhibit moderate absorption, and those with values exceeding 0.2 are characterized by high CNS absorption capacity (24). Furthermore, plasma protein binding (PPB) denotes the extent of interaction between pharmaceutical compounds and various plasma proteins, including human serum albumins (HSAs), present in the bloodstream. This parameter is critical for predicting the pharmacokinetic profile of a drug, particularly in terms of its distribution within the body, and for assessing the proportion of the drug that effectively reaches its target site of action (25).

2.3.3. OSIRIS property explorer

Mutagenicity, tumorigenicity, skin irritability, and reproductive effectiveness assessments of our investigated molecules were completed through the application of the OSIRIS Property Explorer (v.4.5.1), which is a freely downloadable tool (<http://www.organic-chemistry.org/prog/peo/>).

In addition to these assessments, two descriptors, namely drug-likeness (d) and drug score (ds), were also analyzed to support our findings. Therefore, a mathematical approach to the drug-likeness parameter and drug-score evaluation were also implemented, and all results were tabulated in Table 4. Calculation of the drug-likeness (d) of the hit compounds was assessed with Equation 1, where V_i indicates scores of molecular fragments and n denotes the number of molecular fragments.

$$d = \frac{\sum V_i}{\sqrt{n}} \quad (1)$$

Equation 2 is utilized to obtain the drug-score (ds) values of the compounds, where the s_i represents the contributions calculated directly from clogP, logS, molecular weight, and drug-likeness, and t_i represents the contribution taken from the four toxicity risk classes.

$$ds = \pi \left(\frac{1}{2} + \frac{1}{2} s_i \right) \cdot \pi t_i \quad (2)$$

2.3.4. Molinspiration

Along with ADME calculations, potential bioactivities such as G-coupled protein receptor ligand (GPCR), ion-channel modulator (ICM), kinase inhibitor (KI), nuclear receptor ligand (NRL), protease inhibitor (PI), and enzyme inhibitor (KI) were revealed via Molinspiration (<https://www.molinspiration.com>) platform. Notably, G protein-coupled receptors (GPCRs) are an important group of signaling proteins that mediate the responses of cells to a wide range of substances, including hormones, metabolites, cytokines, and neurotransmitters. In addition, ion channels support several cellular functions, including fast cellular rearrangements, heart and skeletal muscle contraction, hormone synthesis, immunological reaction, and tumor cell growth. Furthermore, NRLs are transcription factors that are induced by ligands and, upon translocation to the nucleus, directly influence the transcription of genes, which are essential to several important physiological functions (26). It is essential to note that the assessment of the kinase inhibition (KI) descriptor is of significant importance in determining the bioactivity of the screened candidates against the LIM kinase 1 protein to support the binding scores of our analyzed candidates. The following ranges could be considered in determining the bioactivities: ratings greater than 0.00 indicate substantial bioactivity. Scores that fall within the range of -0.50 to 0.00 represent moderate activity. Bioactivity scores less than -0.50 are considered to indicate inactivity (27).

2.3.5. Syntelly

Syntelly is an online web tool that utilizes artificial intelligence (AI) to accelerate the physicochemical properties, drug-likeness assessments, and toxicity effectiveness of organic compounds. In our study, we have evaluated an alternative perspective on the toxicity profiles of the screened ligands and their drug-likeness properties. For this reason, various toxicity properties, namely Mouse Oral LD₅₀, reproductive toxicity, hepatotoxicity, cardiotoxicity, and carcinogenicity, were predicted to reveal the potential toxicity risks of the investigated candidates.

2.4. Molecular Dynamics

Molecular Dynamics (MD) is a computational simulation commonly employed to evaluate the physical motion of larger molecular systems, with a particular emphasis on protein-ligand complexes. In the most prevalent approach, the trajectories of molecules are ascertained based on Newton's law equations for a system of interacting particles. In this scope, LIMK1: PubChem-136621040, which exhibited the highest docking score, was subjected to MD simulation alongside LIMK1: *native ligand* (PubChem-329823760), serving as the reference protein-ligand complex. The input files of the optimal conformations of these complexes were derived from the docking simulation, and all processes were conducted using the GROningen Machine for Chemical Simulations (GROMACS) 2023.3 software package (28). The preprocessing step was accomplished by selecting the CHARMM36 force field and the TIP3P water model. Subsequently, electrostatic interactions were computed using the

Particle Mesh Ewald (PME) method, with a Fourier spacing of 0.16 nm and a short-range cut-off of 1.2 nm employed for electrostatic treatment. Following the addition of chloride ions to neutralize the system of the complexes, energy minimization was undertaken with 5000 steps of the steepest descent minimization method until the maximum force was less than $10.0 \text{ kJmol}^{-1}\text{nm}^{-1}$. Consequently, system equilibration was performed in two phases, comprising a constant number of particles, volume, and temperature (NVT) ensemble and a continuous number of particles, pressure, and temperature (NPT) ensemble with 5000 steps of steepest descent equilibration. The temperature was escalated within 100 ps in the NVT ensemble and maintained at 300 K with the Berendsen Thermostat to satisfy the room temperature, succeeded by the NPT ensemble at 1 bar for 100 ps. 75 ns MD simulation was completed for both complexes, and corresponding calculations, including root-mean-square deviation (RMSD), root mean square fluctuation (RMSF), solvent-accessible surface area (SASA), and radius of gyration (Rg), were also generated with the GROMACS package to elucidate various dynamic behaviors of our investigated systems.

2.4.1. Root mean square deviation (RMSD) analysis

Root Mean Square Deviation (RMSD) is a metric used to evaluate the average distance between atoms in proteins or ligands that are superimposed after simulation, particularly those that form the backbone. RMSD makes it easier to compare structural differences between different conformational states of proteins or protein-ligand complexes. To calculate the RMSD, the two selected structures must be superimposed. Then, the squared deviation between the coordinates of the respective atoms must be calculated, and the square root of the mean of these squared deviations must be extracted (29). In this context, the conformational stability of complexes during Molecular Dynamics (MD) simulations is often evaluated by the creation of RMSD charts, which may be easily completed with GROMACS.

The following equation (Equation 3) represents the mathematical calculation of RMSD.

$$RMSD = \sqrt{\frac{\sum_{i=1}^N m_i (r_i - r_i')^2}{\sum_{i=1}^N m_i}} \quad (3)$$

2.4.2. Root mean square fluctuation (RMSF) analysis

Root Mean Square Fluctuation (RMSF) is a statistical approach employed to quantify how a particle, including a protein residue, varies from its initial position over a period. It provides important information about areas of a protein that deviate from the typical structure or show the highest degree of flexibility. RMSF is widely used in simulations to identify regions of a protein that exhibit significant flexibility or rigidity (30). RMSF facilitates the evaluation of residue flexibility by helping to identify fluctuating regions during simulations, providing insight into the ways in which ligand binding affects protein flexibility. The formula for computing RMSF is shown in the following equation (Equation 4).

$$RMSF = \sqrt{\frac{1}{N} \sum_j^N (x_{i(j)} - \langle x_i \rangle)^2} \quad (4)$$

2.4.3. Solvent-accessible surface area (SASA) investigation

Surface area of a biological system that is accessible to a solvent is measured by the Solvent-Accessible Surface Area (SASA) method. It is usually computed using a rolling ball algorithm, which examines the molecule's surface using a sphere that represents the solvent of a specific radius (31). The transfer of free energy needed to move a biomolecule from an aqueous solvent to a non-polar solvent, like a lipid environment, is frequently computed using SASA. SASA analysis is especially essential in the context of MD simulations of protein-ligand complexes since it is utilized to estimate the non-polar solvation-free energy, which is a significant part of the protein-ligand complex's binding free energy. The biological activity of the ligand is influenced by the binding free energy, which is a crucial factor in determining the binding affinity between the protein and the ligand. SASA also sheds light on how a ligand interacts with a protein and changes its structure. SASA variations show that the protein is going through significant structural changes in certain areas, which may have an impact on its function. The SASA of the protein-ligand compound is often evaluated during MD simulations at different intervals, providing a real-time view of how the molecule's solvent accessibility changes over time.

2.4.4. Radius of gyration (Rg) assessment

A molecule or a group of atoms can be evaluated for size and structure using the radius of gyration (Rg). It offers a view of the molecule's general shape and spatial extent by revealing the distribution of mass with respect to its center of mass. Rg can be used to monitor conformational changes, such as those that occur during folding or unfolding events, or to characterize the compactness of a molecular structure over time (32). By quantifying this dispersion, Rg helps characterize the compactness, flexibility, and conformational changes of macromolecules during the MD simulation. It offers important details about the size and shape of macromolecules and their dynamics. Mathematically, Rg is defined as the root mean square distance of each particle from the center of mass in Equation 5.

$$Rg = \sqrt{\frac{1}{N} \sum_{i=1}^N m_i \cdot r_i^2} \quad (5)$$

3. RESULTS AND DISCUSSION

3.1. Molecular Docking Studies

3.1.1. Docking validation

Docking validation was initially completed to verify our specified docking methodology. This was achieved by removing the native ligand from the crystal structure and conducting a molecular docking simulation with the same compound, a process known as redocking. The original compound (depicted in green) was then superimposed with the docked compound (shown in blue), and the Root Mean Square Deviation (RMSD) value, measuring the

difference between these two conformations, was determined to be 1.6 Å (Figure 2).

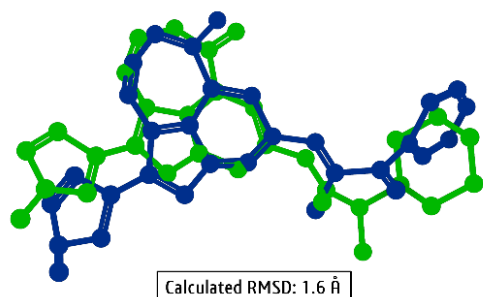
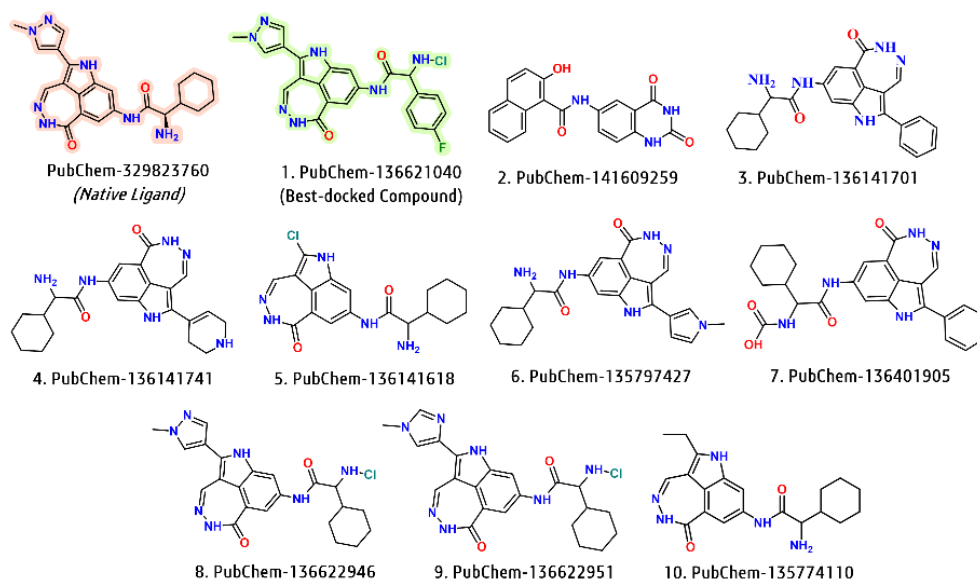


Figure 2: Superimposition of the redocked PubChem-329823760 (*blue*) onto its initial conformation in the active site of LIMK1 (RMSD: 1.6Å).

3.1.2. Docking results

The main purpose of this analysis is to conduct an extensive molecular docking investigation to assess the inhibitory potential of 30 candidate drugs against the LIMK1 receptor (PDB ID: 5NXC). The binding scores of the top 10 ligands, which exhibited the highest binding affinity to the macromolecule, are presented in Table 1, accompanied by the 2D structures of the analyzed ligands. Figure 3, in addition, provides a visual representation of the binding poses and residue interactions between LIMK1 and the best-docked ligand (PubChem-136621040). Moreover, the binding pose and residue interaction of LIMK1 with the native ligand were also depicted. Docking scores, binding poses, and residue interactions of the remaining 20 virtual hits were given in electronic supplementary material in Table S5-S6, and Figure S6, respectively.

Table 1: Docking scores and 2D structure representations of the top 10 ligands.



PubChem ID	Docking Scores (kcal/mol)
329823760 (<i>Native ligand</i>)	-9.80
136621040	-10.60
141609259	-10.10
136141701	-10.00
136141741	-10.00
136141618	-9.80
135797427	-9.60
136401905	-9.50
136622946	-9.50
136622951	-9.50
135774110	-9.30

Our findings have revealed that the binding affinities of the 30 screened molecules ranged from -5.20 to -10.60 kcal/mol. Among these 30 virtual hits, docking scores of the top 10 compounds were specifically selected to evaluate their binding potentials. For the top-ranked four ligands, specifically PubChem-136621040 (-10.60 kcal/mol), PubChem-141609259 (-10.10 kcal/mol), PubChem-136141701 (-10.00 kcal/mol), and PubChem-136141741 (-10.00 kcal/mol), exhibited relatively higher binding affinities in comparison with the native ligand {PubChem-136621040 (-9.80 kcal/mol)}. In

addition, PubChem-136141618 (-9.80 kcal/mol) showed an identical binding potential with the reference ligand. Subsequently, the remaining compounds including, PubChem-135797427 (-9.60 kcal/mol), PubChem-136401937 (-9.60 kcal/mol), PubChem-136401905 (-9.50 kcal/mol), PubChem-136622946 (-9.50 kcal/mol), and PubChem-136622951 (-9.50 kcal/mol) demonstrated lower binding potentials, indicating weaker binding interactions with the residues of LIMK1 receptor (Figure 3).

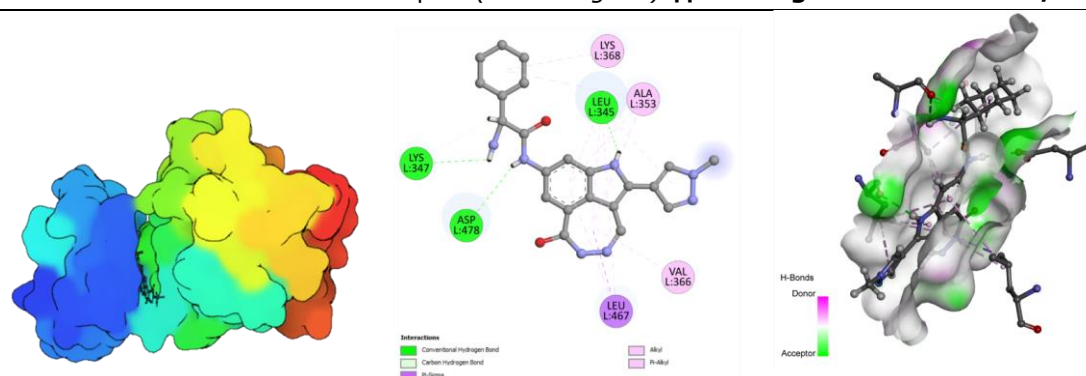
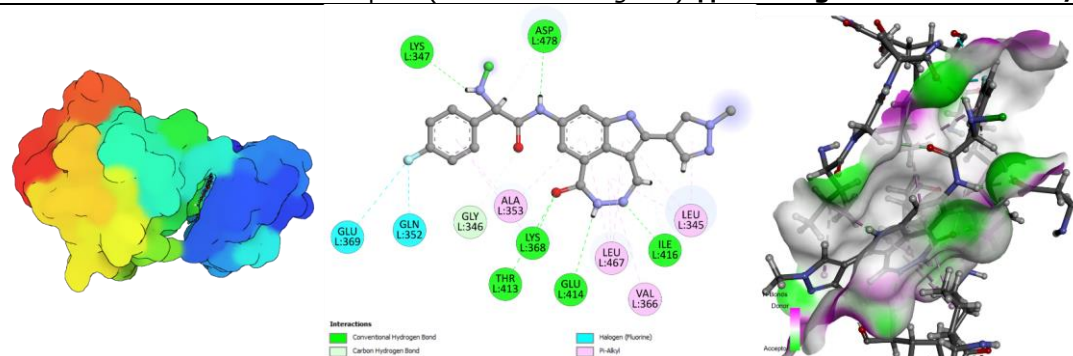
PubChem-329823760: LIMK1 complex (*Native Ligand*) || Binding score: -9.80 kcal/molPubChem-136621040: LIMK1 complex (*Best-docked Ligand*) || Binding score: -10.6 kcal/mol

Figure 3: Binding poses and residue interactions of the native and the screened ligand with LIMK1 (PDB ID: 5NXC).

It is crucial to state that the highest-ranked compound that possessed -10.60 kcal/mol has shown relatively greater binding affinity among these virtual hits in terms of its docking score. Therefore, we have also checked the patent status of the compound. The findings revealed that the molecule had been previously identified in a patent document as an inhibitor of checkpoint kinase 1 (CHK-1 or p56CHK-1), a member of the kinase family. With respect to the binding poses and residue interactions of the native ligand LIMK1 complex (PubChem-329823760), the diazepinoindole subunit of the compound was found to interact with a variety of amino acid residues, including LEU345, LEU467, ALA353, and VAL366. A range of intermolecular interactions were identified between the ligand and the residues, encompassing hydrogen bond interactions, pi-alkyl interactions, and pi-sigma interactions. Various hydrogen bond interactions were also observed with several residues, namely LYS347, LYS368, and ASP478. Our analyzed compound, which exhibited the highest docking score (PubChem-136321040), demonstrated a greater number of residue interactions with the LIMK1 receptor. The diazepinoindole fragment of the ligand showed a higher degree of residue interactions, including various hydrogen bond interactions with residues LYS368, THR413, GLU414, and ILE416, in addition to pi-alkyl interactions with residues ALA353, LEU345, LEU467, and VAL366. Other interactions were observed with residues LYS347 and ASP478. Hydrogen bond interactions were also detected with these two amino acids. Additionally, the substitution of the fluorobenzene unit in our compound with the cyclohexyl fragment

present in the structure of the native ligand enabled the formation of interactions with an increased number of amino acids, including the halogen interactions with GLU352 and GLU369. This could consequently lead to an increase in the docking score of this ligand.

3.2. Prediction of ADMET, Drug-likeness and Pharmacokinetic Properties

3.2.1. SwissADME analysis

SwissADME server was employed to elucidate the pharmacological characteristics of our potential inhibitory agents against the LIMK1 receptor. Within this context, the results for the top 10 compounds were listed in Table 2, whereas the data for the remaining 20 compounds can be found in Table S1 in the electronic supplementary information (ESI[†]). The evaluation process was guided by Lipinski's rule of five. All the compounds demonstrated molecular weights under 500 Da, thereby satisfying the set benchmark. Furthermore, the analysis of hydrogen bond acceptors (HBA) and hydrogen bond donors (HBD) was in accordance with the rule of five, suggesting the compounds possess desirable drug-like characteristics. Analysis of the number of rotatable bonds (nROTB), highly influencing molecular flexibility, revealed that our candidate compounds adhered to the ideal pharmaceutical limit of 9. Importantly, all candidate compounds exhibited topological polar surface area (TPSA) values that were below the threshold of 140 Å², which is indicative of favorable drug absorption potential. Therefore, the majority of our candidate compounds demonstrated a high potential for gastrointestinal absorption. However, four compounds, namely

PubChem-136401905, PubChem-135774106, PubChem-136181657, and PubChem-135794603, were exceptions to this trend. Consensus $\log P_{o/w}$ was

also assessed to evaluate lipophilicity, and all the molecules that ranged from -0.79 to 3.69 showed the desired values that obey Lipinski's rule.

Table 2: ADME Results of the top 10 candidate pharmaceuticals possessing the highest docking scores.

PubChem ID	^a MW (Da)	^b HBA	^c HBD	^d nROTB	^e TPSA (\AA^2)	^f GI abs.	^g BBB	^h clogP _{o/w}	Sol.	Violation
329823760	419.48	5	4	5	134.48	High	No	2.85	PS	0
136621040	465.87	6	4	6	120.49	High	No	2.54	S	0
141609259	347.32	4	4	3	115.05	High	No	2.39	MS	0
146582701	262.29	3	4	3	115.34	High	No	0.57	S	0
136141741	420.51	5	5	5	128.69	High	No	2.22	S	0
136141618	373.84	4	4	4	116.66	High	No	2.54	S	0
135797427	418.49	4	4	5	121.59	High	No	2.56	S	0
136401905	459.50	5	5	7	139.97	Low	No	3.19	MS	0
136622946	453.92	5	4	6	120.49	High	No	2.58	MS	0
136622951	453.92	5	4	6	120.49	High	No	2.45	MS	0
135774110	367.44	4	4	5	116.66	High	No	2.61	S	0

Lipinski's Rule: ^aMW \leq 500g/mol, ^bHBA \leq 10, ^cHBD \leq 5, ^dnROTB \leq 9, ^eTPSA \leq 140 \AA^2 , ^fclogP_{o/w} \leq 5

Abbreviations: ^aMW: Molecular Weight, ^bHBA: Hydrogen Bond Acceptor, ^cHBD: Hydrogen Bond Donor, ^dnROTB: Number of Rotatable Bonds, ^eTPSA: Topological Polar Surface Area, ^fGI abs: Gastrointestinal absorption, ^gBBB: Blood-brain Barrier Permeability, ^hclogP_{o/w}: Consensus ^hclogP_{o/w}, IS: Insoluble, PS: Poorly Soluble, MS: Moderately Soluble, S: Soluble, HS: Highly Soluble.

Among these parameters, the descriptor that assesses blood-brain barrier permeability (BBB) that determines whether the investigated compounds permeate the central nervous system (CNS) plays a critical role in the development of novel drug molecules against Alzheimer's Disease. It was deduced from SwissADME findings that our screened candidates possessed no BBB permeability. Given that these initial calculations did not yield definitive results, particularly in terms of quantifying BBB permeability, we intended to elucidate the CNS permeability of our using additional in silico platforms, which were discussed in the following section.

We have also employed the BOILED-Egg (Brain or Intestinal Estimated Permeation) graphical tool, integrated within the SwissADME platform, to evaluate the passive permeability of the blood-brain barrier, represented by the yellow region, and the passive gastrointestinal absorption (HIA), represented by the white region. These assessments are based on the positioning of the molecules, calculated using the total area of the WLOGP versus TPSA (Wildman & Crippen, 1999). The BOILED-Egg representation of our analyzed pharmaceuticals is given in Figure 4.

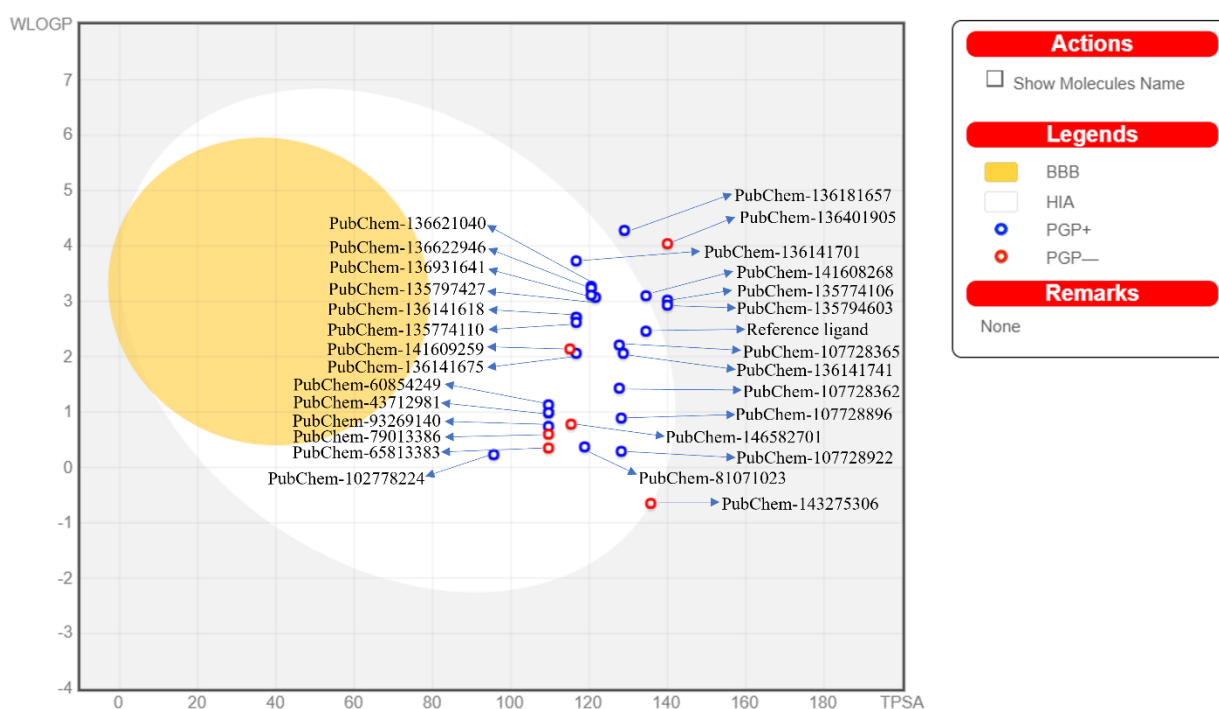


Figure 4: BOILED-EGG representation: Prediction of passive gastrointestinal absorption and passive brain penetration of candidate molecules.

The prediction of P-glycoprotein (P-gp) substrates is crucial, as it is the primary active efflux mechanism implicated in various biological barriers, including the blood-brain barrier. This could be visually represented and evaluated through a color-coded graphical depiction. Passive absorption is indicated by the positioning within or outside the white zone, while passive brain access is denoted by the positioning within or outside the yellow region. The active efflux from the central nervous system or into the gastrointestinal lumen is represented by color-coding: blue dots for P-gp substrates (PGP⁺) and red dots for non-P-gp substrates (PGP⁻). From the graphical representation, it is evident that the majority of our molecules, including PubChem-329823760 (the reference ligand) and PubChem-136621040 (which has the highest docking score against the receptor), are located within the white region of the egg. This suggests that the gastrointestinal system could passively absorb these compounds.

Conversely, several compounds, namely PubChem-136181657, PubChem-136401905, PubChem-141608268, and PubChem-135794603, were unable to traverse the gastrointestinal system passively. As a result, no passive permeation of the BBB was observed with our candidate compounds. Interestingly, compounds denoted as blue dots (PGP⁺) have successfully crossed the central nervous system actively, while those denoted with red dots (PGP⁻) were unable to permeate the CNS actively. Excluding PubChem-136141675, PubChem-79013386, PubChem-65813383, PubChem-146582701, PubChem-143275306, and PubChem-136401905, our compounds have successfully

crossed the CNS, including our best-docked compound (PubChem-136621040) and the native ligand.

Bioavailability radars serve as valuable tools for visually presenting computed physicochemical and pharmacological attributes of potential drug candidates concerning oral drug characteristics, offering insights into their potential oral bioavailability. These radars depict parameters including lipophilicity (LIPO), molecular weight (SIZE), polarity (POLAR), insolubility (INSOLU), unsaturation (INSATU), and flexibility (FLEX). Figure 5 illustrates the bioavailability radars of a reference ligand (PubChem-329823760) and the ligand exhibiting the highest binding affinity (PubChem-136621040) against LIMK1. Parameters crucial for the oral bioavailability of our lead molecule, characterized by the highest docking score, fell within the desired range except for saturation in comparison to the reference ligand. Saturation, delineated by the proportion of carbons in sp³ hybridization within the molecule, ideally falls between 0.25 and 1.

However, a saturation value of 0.09 was observed for our compound, resulting in a deviation from the designated pink hexagonal region. Radar representations of other scrutinized ligands are available in the supplementary material (ESI⁺). These radar plots similarly indicate that the oral availability potential of these candidate molecules conforms to an ideal trend, falling within the pink hexagonal area, except for PubChem-136141701, where the saturation value deviates from the ideal, akin to the highest-docked compound.

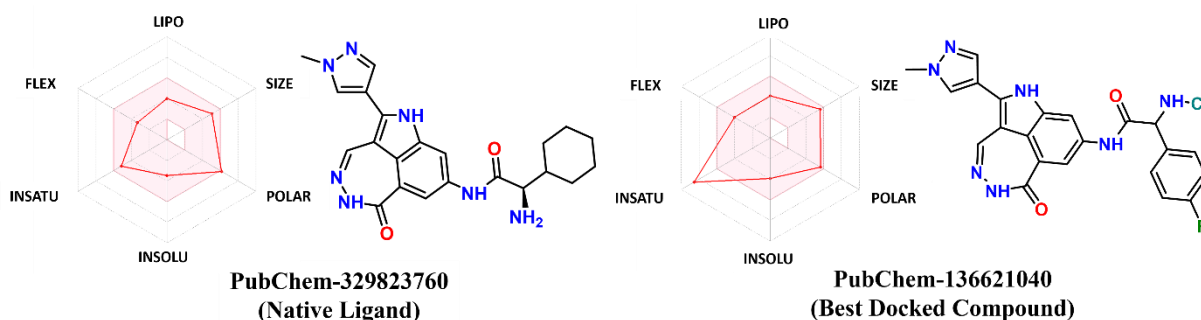


Figure 5: Bioavailability radar representations and structures of the native ligand and best-docked compound.

3.2.2. PreADMET calculations

Our findings showed that most of the candidate pharmaceuticals exhibited substantial absorption capabilities through the central nervous system (CNS) and, consequently, the blood-brain barrier (BBB), with values ranging from 0.01 to 0.35. The native ligand, in comparison, showed a relatively lower absorption with a BBB value of 0.12. Notably, our top-docked compound demonstrated a BBB value of 0.20, indicating its high absorption potential through the BBB. We have also evaluated the passive gastrointestinal absorption, denoted as HIA, and plasma-protein binding (PPB) capacities of our

compounds. The majority of compounds exhibited over 70% passive absorption through the gastrointestinal system except PubChem-143275306 (44.70%), PubChem-107728922 (46.96%), and PubChem-107728896 (49.31%). Specifically, PubChem-136621040 (the best-docked molecule) displayed an impressive HIA value of 89.50%, while the native ligand (PubChem-136621040) had a value of 82.70%. The PPB capacities of our compounds varied from 0.00% to 92.24%. Our compound demonstrated a significantly higher plasma-protein binding capacity (88.00%) compared to the native ligand, which had a value of 50.95% (Table 3).

Table 3: Various ADME profiles of the top 10 compounds with the highest binding affinities.

PubChem ID	BBB ^a ([brain]/[blood])	HIA ^c (%)	PPB ^e (%)
329823760	0.12	82.70	50.95
136621040	0.20	89.50	88.00
141609259	0.04	90.80	78.70
146582701	0.53	87.11	87.29
136141741	0.15	78.64	28.05
136141618	0.22	83.67	46.55
135797427	0.27	85.50	64.53
136401905	0.34	83.45	84.98
136622946	0.35	87.75	86.05
136622951	0.30	87.74	82.83
135774110	0.29	80.76	56.29

Abbreviations: ^aBBB: Blood-brain barrier, ^cHIA: Passive gastrointestinal absorption, ^ePPB: Plasma-protein binding

The rule for BBB permeability: <0.1 low absorption by CNS, between 0.1 and 0.2 moderate absorption, >0.2 high absorption

3.2.3. OSIRIS property explorer analysis

Toxicity risk factors of the compounds, including mutagenicity, tumorigenicity, skin irritability, and reproductive effectiveness, were evaluated using OSIRIS software. Additionally, the studied ligands' drug-likeness characteristics and drug scores were assessed to assess the compounds further, and the results of the top 10 compounds possessing the highest docking scores were illustrated in Table 4. The results of the remaining screened candidates were provided in Table S2 in the electronic supplementary information (ESI⁺).

In the context of mutagenicity assessment, select compounds, namely PubChem-136621040, PubChem-136622946, PubChem-136622951, PubChem-135774106, and PubChem-135794603, demonstrated moderate toxicity, while PubChem-141609259, PubChem-136141701, PubChem-136401905, and PubChem-146582701 exhibited high toxicity. Conversely, the remaining ligands exhibited negligible toxicity. Remarkably, the initial 18 ligands, characterized by the highest binding affinities, displayed significant tumorigenic potential, contrasting with the absence of toxicity indications in

other ligands. Moreover, PubChem-136141701, PubChem-136401905, and PubChem-141608268 exhibited notable irritancy and reproductive toxicity, while others showed minimal to no such effects. Regarding drug-likeness (d), the compound with the best binding score (PubChem-136621040) showcased the highest value at 7.46, surpassing the reference ligands' 1.34, with other ligands ranging from -52.96 to +4.07. Notably, most investigated ligands exhibited superior drug-likeness compared to the reference. Additionally, drug-score values, which is another mathematical approach used to calculate pharmacological features of the studied compounds, ranged from 0.05 to 0.78.

3.2.4. Molinspiration studies

Bioactivity scores and pharmacological aspects of the compounds were also investigated using the Molinspiration Property Calculation tool. Table 5 presents the bioactivity scores of the ligands, and drug-likeness analysis results are listed in Table 6. The remaining results were tabulated in the electronic supplementary information (ESI⁺) in Table S5 and Table S6.

Table 4: Toxicity results of the studied candidates.

PubChem ID	Mut	Tum	Irr.	Rep. E.	d	ds
329823760	●	●	●	●	+1.34	0.33
136621040	●	●	●	●	+7.46	0.27
141609259	●	●	●	●	-2.64	0.12
136141701	●	●	●	●	+0.55	0.05
136141741	●	●	●	●	+0.85	0.32
136141618	●	●	●	●	+0.50	0.31
135797427	●	●	●	●	+1.24	0.33
136401905	●	●	●	●	+3.26	0.05
136622946	●	●	●	●	+3.74	0.25
136622951	●	●	●	●	+4.07	0.28
135774110	●	●	●	●	+0.68	0.32

Abbreviations: Mut: Mutagenic, Tum: Tumorigenic, Irr: Irritation, Rep. E: Reproductive effectiveness, d: Drug-likeness, ds: Drug Score

● No detectable toxicity ● Moderate toxicity ● High toxicity

Table 5: Bioactivity calculations against several receptors of the top 10 molecules with the best docking scores.

PubChem ID	GPCR	ICM	KI	NRL	PI	EI
329823760	0.04	-0.14	0.40	-0.88	-0.04	0.19
136621040	-0.12	-0.30	0.29	-0.72	-0.38	-0.02
141609259	-0.03	-0.25	0.05	-0.20	-0.14	0.04
136141701	0.05	-0.03	0.31	-0.52	0.05	0.23
136141741	0.20	0.09	0.34	-0.51	0.07	0.31
136141618	0.10	0.04	0.31	-0.67	0.07	0.25
135797427	0.14	-0.03	0.51	-0.41	-0.08	0.34
136401905	0.13	0.00	0.19	-0.40	0.15	0.25
136622946	-0.04	-0.17	0.28	-0.81	-0.23	0.07
136622951	0.17	0.04	0.45	-0.44	-0.01	0.35
135774110	-0.02	-0.06	0.22	-0.67	-0.01	0.20

Abbreviations: GPCR: G protein-coupled receptor ligands, ICM: Ion Channel Modulator, KI: Kinase Inhibitor, NRL: Nuclear Receptor Ligand, PI: Protease Inhibitor, EI: Enzyme Inhibitor

Various bioactivity descriptors were effectively computed using the Molinspiration platform, including G protein-coupled receptor ligands (GPCRL), ion-channel modulators (ICM), kinase inhibitors (KI), nuclear receptor ligands (NRL), protease inhibitors (PI), and enzyme inhibitors (EI). As discussed, a bioactivity score exceeding 0.00 denotes significant bioactivity, while values within the range of -0.50 to 0.0 indicate moderate bioactivity, and those below -0.50 indicate a lack of bioactivity. The GPCR inhibitory activity values for these compounds ranged from -0.12 to +0.46, demonstrating bioactivity levels ranging from moderate to significant. Similarly, ICM values varied from -0.30 to +0.24, indicating moderate or

significant bioactivity against ion-channel modulators. NRL capabilities were relatively lower compared to other descriptors, with values ranging from -0.92 to -0.01, suggesting either a lack of bioactivity or moderate bioactivity for certain compounds. Protease and enzyme inhibitory activity also ranged from moderate to high, with values spanning from -0.38 to +0.48 and -0.02 to +0.48, respectively. Notably, kinase inhibition capability emerged as the most crucial descriptor for our investigated candidates, with the top 10 compounds effectively inhibiting kinase proteins, including LIM kinase proteins, with values ranging from -0.66 to +0.51.

Table 6: ADME Assessments of the top 10 ligands having the highest docking score.

PubChem ID	mi-LogP ^a	TPSA ^b	nAtoms ^c	nON ^d	nOHNH ^e	nROTB ^f	Volume	Violation
329823760	1.25	134.49	31	9	5	4	375.50	0
136621040	2.21	120.50	33	9	4	5	376.50	0
141609259	2.60	115.05	26	7	4	2	290.78	0
136141701	2.87	116.67	31	7	5	4	377.73	0
136141741	1.24	128.69	31	8	6	4	385.70	1
136141618	2.00	116.67	26	7	5	3	319.86	0
135797427	1.78	121.60	31	8	5	4	379.66	0
136401905	4.82	139.97	34	9	5	5	405.85	0
136622946	2.74	120.50	32	9	4	5	390.15	0
136622951	2.30	120.50	32	9	4	5	390.15	0
135774110	2.00	116.67	27	7	5	4	339.69	0

Abbreviations: ^amiLogP: Partition coefficient between n-octanol and water (logP_{o/w}), ^bTPSA: Topological polar surface area, ^cnAtoms: Number of atoms, ^dnON: Number of hydrogen bond acceptors (HBA), ^enOHNH: Number of hydrogen bond donors (HBD), ^fnROTB: Number of rotatable bonds

Likewise, ADME analyses were conducted using the Molinspiration platform to corroborate the previous findings obtained from OSIRIS and SwissADME. Thus far, parameters including Hydrogen Bond Acceptors (HBA), Hydrogen Bond Donors (HBD), and the number of Rotatable Bonds (nROTB) have been

determined to adhere to Lipinski's rule, indicating favorable drug-likeness. Furthermore, the lipophilic characteristics of the candidate compounds, assessed through miLogP values, were within the prescribed range, with all compounds falling below the upper limit of miLogP (5), thereby aligning with

Lipinski's rule. This comprehensive evaluation underscores the compatibility of the identified hits with established criteria for drug development, further validating their potential as viable therapeutic candidates.

3.2.5. Syntelly calculations

Several toxicity characteristics of our candidate pharmaceuticals were assessed through the Syntelly platform, an online AI-powered compound characterization tool. In this scope, mouse oral LD₅₀, hepatotoxicity, cardiotoxicity, and carcinogenicity characteristics of our investigated compounds were

calculated. The findings suggest that the LD₅₀ values of our target molecules ranged from 745 to 2320 mg/kg. The compound PubChem-141609259 exhibited the highest LD₅₀ value, indicating relatively lower toxicity in mice. The compound with the highest docking score exhibited an LD₅₀ value of 784 mg/kg, compared to the native ligand's LD₅₀ value of 920 mg/kg. All the investigated compounds showed signs of reproductive toxicity, but none displayed cardiotoxicity. The top-docked conformation was found to be hepatotoxic; however, no signs of carcinogenicity were observed (Table 7).

Table 7: Toxicity assessments of the investigated compounds.

PubChem ID	M.O LD ₅₀ (mg/kg)	Rep. Tox.	Hpt.	Crd.	Crn.	Tox	Phys	Bio	Eco
329823760	920.00	T	NT	NT	NT	●	●	●	●
136621040	784.00	T	T	NT	NT	●	●	●	●
141609259	2320.00	T	T	NT	NT	●	●	●	●
136141701	946.00	T	NT	NT	NT	●	●	●	●
136141741	650.00	T	NT	NT	NT	●	●	●	●
136141618	1280.00	T	NT	NT	NT	●	●	●	●
135797427	1040.00	T	NT	NT	NT	●	●	●	●
136401905	2130.00	T	T	NT	NT	●	●	●	●
136622946	796.00	T	NT	NT	NT	●	●	●	●
136622951	847.00	T	T	NT	NT	●	●	●	●
135774110	745.00	T	NT	NT	T	●	●	●	●

Abbreviations: M.O. LD₅₀: Mouse oral LD₅₀, Rep. Tox: Reproductive toxicity, Hpt: Hepatotoxicity, Crd: Cardiotoxicity, Crn: Carcinogenicity, T: Toxic, NT: Non-toxic, logBB: Logarithmic value of blood-brain barrier permeability

3.3. Molecular Dynamics Simulations

Molecular dynamics simulations were implemented utilizing GROningen Machine for Chemical Simulations (GROMACS) 2023.3 software package to investigate the binding stability of the selected complexes during the simulation. In this scope, MD simulations of PubChem-329823760: LIMK1 (native ligand) and PubChem-136321040: LIMK1 (best-docked compound: LIMK1) complexes were carried out to analyze the binding stabilities during the simulation better. For this reason, root mean square deviation (RMSD), root mean square fluctuation (RMSF), solvent-accessible surface area (SASA), and radius of gyration (Rg) analyses were calculated using the trajectories and corresponding graphs were illustrated in Figure 6-9.

3.3.1. Root mean square deviation (RMSD) analysis

In the evaluation RMSD results, the complex PubChem-329823760: LIMK1 exhibited an average RMSD value of 0.31 nm, while the apo form registered an average of 0.29 nm. Minor fluctuations were observed in both the complex and the apo form in the interval from 10 ns to 25 ns. A notable fluctuation was discerned in the complex around the 40th ns, with an RMSD value approximating 0.50 nm. Concurrently, the apo form was found to be more stable than the complex, with its fluctuation ranging between 0.20 and 0.30 nm. Post the 40 ns mark, both the complex and the apo form were observed to attain relative stability, which was maintained throughout the remaining duration of the simulation (Figure 6).

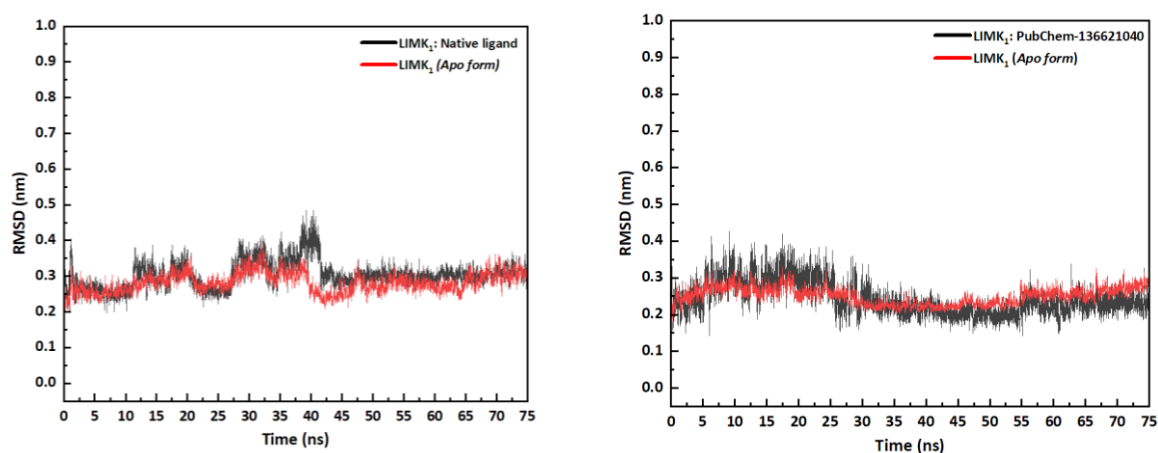


Figure 6: RMSD trajectory plots of PubChem-329823760: LIMK1 (*native ligand*) and PubChem-136621040: LIMK1 (*best-docked*) complexes with their corresponding Apo forms.

Additionally, the complex, including our target compound, exhibited an average RMSD value of 0.23 nm, while the apo form of this complex showed an RMSD of 0.26 nm. This could be interpreted as a sign of the relative stability of our screened candidate during the MD simulation in the binding site of LIMK1. In the initial 25 ns, a slight fluctuation was observed in both the complex and the apo form. During these stages, the complex demonstrated a slightly more substantial fluctuation. However, stability was observed to be achieved subsequent to the 30 ns threshold. The apo form did not present any significant fluctuations, and a state of equilibrium was sustained in the system for the remainder of the simulation period.

3.3.2. Root mean square fluctuation (RMSF) analysis

The computation of RMSF for the trajectories of the complexes PubChem-329823760: LIMK1 (native

ligand) and PubChem-136321040: LIMK1 (best-docked) is depicted in Figure 7. This illustration provides insight into the adaptability of the respective ligands within the receptor network and the mobility of residues within the LIMK1 macromolecule's binding site. A lower RMSF fluctuation is typically indicative of a flexible complex characterized by a rigid protein secondary structure, while a higher RMSF value suggests a relatively weaker bonded structure. The application of C_{α} atoms facilitated a more comprehensive understanding of each residue's average position. The RMSF value for the complex with the native ligand (PubChem-329823760: LIMK1) was determined to be approximately 0.12 nm, while the average RMSF for the highest-ranked complex (PubChem-136321040: LIMK1) was found to be 0.10 nm (Figure 7).

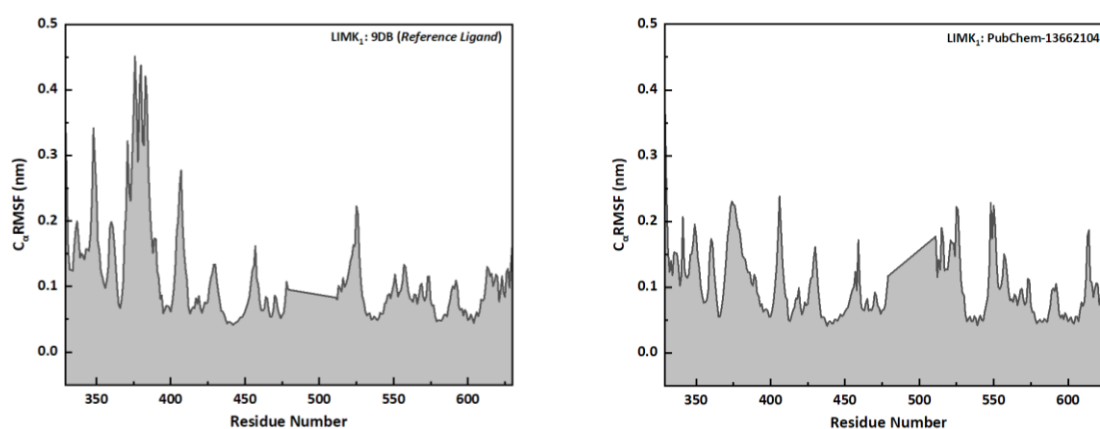


Figure 7: C_{α} RMSF plots of PubChem-329823760: LIMK1 (native ligand) and PubChem-136321040: LIMK1 (best-docked) complexes.

In the residue number range of approximately 350 to 450, substantial fluctuations were observed. Specifically, a significant peak of about 0.45 nm was discerned around residues 375 and 400, suggesting an enhanced interaction between the native ligand and these residues. Minor peaks, each approximately 0.15 nm, were identified between residues 425 and 450. Another peak of note was also identified around residues 520 and 525, with an approximate value of 0.25 nm. Additionally, a series of minor residue fluctuations were detected in the range from 550 to 650 residue numbers, most of which were around 0.10 nm.

A comparatively lower RMSF value with minor peaks was noted for the top-ranked ligand (PubChem-136321040: LIMK1). Specifically, more subtle fluctuations were observed between residue numbers 350 and 450, in contrast to the complex with the native ligand. Two similar peaks were also detected around residues 425 and 450. For these complexes, relatively higher fluctuations were observed in the range of 500 to 650, with various peaks at residues 525, 550, and 610 with an RMSF value of 0.20 nm and a minor fluctuation around residue 580 at approximately 0.10 nm.

3.3.3. Solvent-accessible surface area (SASA) calculation

Solvent Accessible Surface Area is a measure of the surface area of a protein-ligand complex that is directly engaged in interactions with solvent molecules. An increase in SASA values implies a more unfolded or open conformation, signifying a higher degree of exposure to the solvent (33). During 75 ns MD simulation, the average SASA values of the complexes PubChem-329823760: LIMK1 (native ligand) and PubChem-136321040: LIMK1 (best-docked) were observed. The native ligand LIMK1 complex displayed an average SASA value of approximately 150.80 nm², while the best-docked compound, LIMK1, exhibited a nearly identical average value of 150.20 nm². Notably, the complex containing the native compound demonstrated relatively more stability during the first 40 ns.

In contrast, the fluctuation of the complex with the best-docked compound slightly decreased between 30 and 50 ns. Both complexes showed nearly identical fluctuations until the end of the trajectories. Minor fluctuations were noted in the trajectory of the PubChem-136321040: LIMK1 complex between 50 and 75 ns. These comprehensive SASA analyses suggest that both complexes interacted with a similar quantity of solvents throughout the MD simulation (Figure 8).

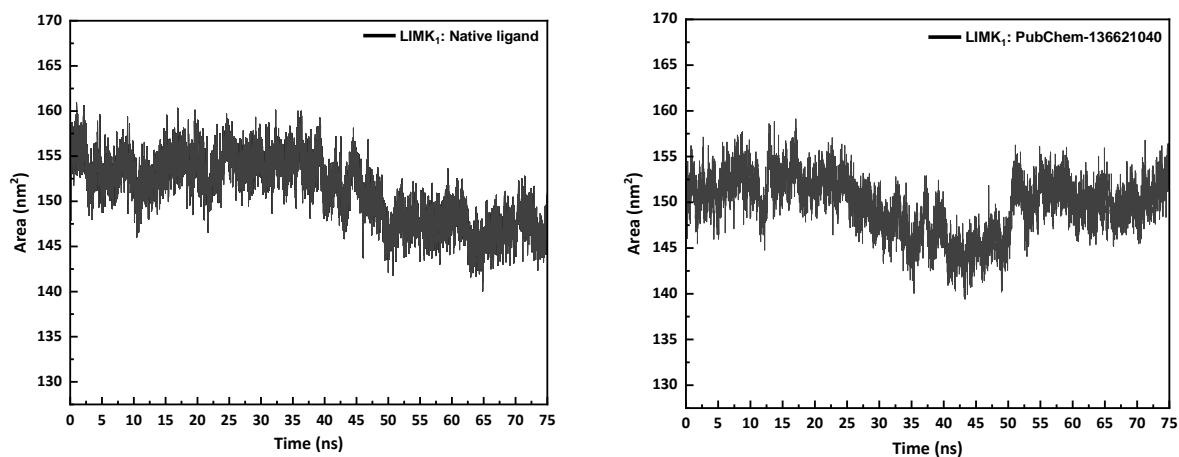


Figure 8: SASA trajectories of PubChem-329823760: LIMK1 (*native ligand*) and PubChem-136321040: LIMK1 (*best-docked*) complexes.

3.3.4. Radius of gyration (*Rg*) analysis

The calculation of the radius of gyration was employed to assess the compactness and rigidity of the macromolecule throughout the MD simulation. The trajectories of *Rg* versus time for our complexes are depicted in Figure 9. The average *Rg* values were determined to be 2.06 nm and 2.04 nm for the PubChem-329823760: LIMK1 and PubChem-

136321040: LIMK1 complexes, respectively. In the initial 20 ns, both complexes exhibited a similar trend, indicative of the molecule's stable compactness at the onset of the simulation. Subsequently, the fluctuation of the native compound complex increased from approximately 2.05 nm to 2.10 nm between 30 and 40 ns.

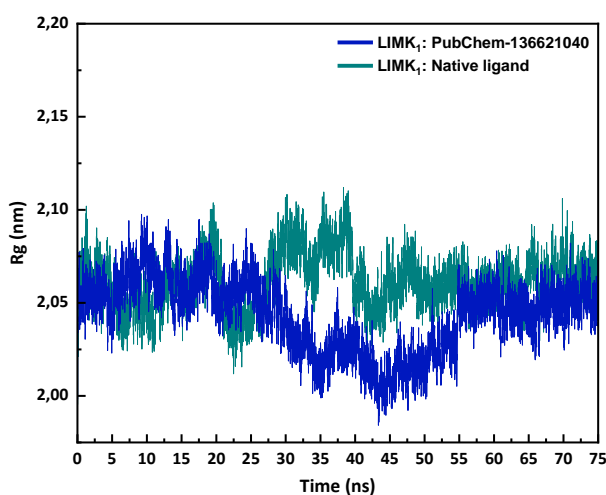


Figure 9: Radius of gyration graphs of PubChem-329823760: LIMK1 (*native ligand*) and PubChem-136321040: LIMK1 (*best-docked*) complexes.

In comparison, the fluctuation of the complex containing our candidate compound slightly decreased from 2.05 nm to around 2.00 nm from 30 ns to 45 ns before this trend slightly increased again and reached equilibrium from 55 ns to 75 ns. The native ligand-LIMK1 complex achieved equilibrium after a significant fluctuation at about 45 ns and maintained its stability for the duration of the simulation. It could be deduced from both complexes that these protein systems maintained their rigidity during the simulation, based on the average results, as discussed above.

4. CONCLUSION

In this study, we successfully identified several candidate compounds possessing the inhibitory potential against LIM domain kinase 1 receptor, playing a pivotal role in Alzheimer's Disease (AD).

PubChem database through Pharmit server was utilized to conduct pharmacophore-based virtual screening to determine similar structures. 419 compounds were discovered at initial, and 29 hit compounds were identified by applying pharmacophore filter and Lipinski's filter.

PubChem-136621040 stood out as particularly promising, exhibiting not only a high binding affinity but also favorable pharmacokinetic and ADMET profiles, as evidenced by comprehensive *in silico* analyses encompassing molecular docking, dynamic simulations, and ADMET predictions.

The docking results corroborated the compound's superior binding affinity for LIMK1 relative to the native ligand, as indicated by a significantly elevated docking score, thereby highlighting its potential as a highly effective inhibitor. The 75 ns MD simulations

offered detailed insights into the interactions between the LIMK1 enzyme and the identified inhibitors. RMSD analysis revealed that PubChem-136621040 maintained a lower average RMSD value of 0.23 nm compared to the native ligand's 0.31 nm, indicating a stable interaction throughout the simulation. RMSF analysis further corroborated these findings, showing that PubChem-136621040 had a lower average RMSF value, suggesting a stable and consistent interaction with key residues within the LIMK1 binding site. The SASA and radius of gyration (Rg) analyses offered further understanding of the dynamic behavior of the ligand-enzyme complexes. The SASA values, approximately 150 nm² for both the native ligand and PubChem-136621040, suggested stable solvation properties during the simulation. Concurrently, the Rg analysis revealed that both complexes preserved their structural integrity and compactness, with PubChem-136621040 exhibiting a modest increase in rigidity relative to the native ligand.

These findings will enhance the expanding research on LIMK1 inhibitors for Alzheimer's disease treatment and set the stage for subsequent *in vitro* and *in vivo* validation studies, structure-activity relationship analyses, and investigations into potential synergistic effects with other AD therapies. This study exemplifies the effectiveness of combining various computational approaches in drug discovery and establishes a robust basis for the development of innovative therapeutic strategies for AD.

5. CONFLICT OF INTEREST

The authors affirm that there are no competing financial interests or personal relationships known to them that might seem to affect the integrity of the work presented in this paper.

6. ACKNOWLEDGMENTS

The computational calculations were executed at TUBITAK-ULAKBIM High Performance and Grid Computing Centre (TRUBA).

7. REFERENCES

1. Breijyeh Z, Karaman R. Comprehensive Review on Alzheimer's Disease: Causes and Treatment. *Molecules* [Internet]. 2020 Dec 8;25(24):5789. Available from: [<URL>](#).
2. Cummings JL. Alzheimer Disease. *JAMA* [Internet]. 2002 May 8;287(18):2335. Available from: [<URL>](#).
3. Brookmeyer R, Evans DA, Hebert L, Langa KM, Heeringa SG, Plassman BL, et al. National estimates of the prevalence of Alzheimer's disease in the United States. *Alzheimer's Dement* [Internet]. 2011 Jan 1;7(1):61–73. Available from: [<URL>](#).
4. Gomez-Arboledas A, Davila JC, Sanchez-Mejias E, Navarro V, Nuñez-Díaz C, Sanchez-Varo R, et al. Phagocytic clearance of presynaptic dystrophies by reactive astrocytes in Alzheimer's disease. *Glia*

- [Internet]. 2018 Mar 27;66(3):637–53. Available from: [<URL>](#).
5. Sharoar MG, Hu X, Ma XM, Zhu X, Yan R. Sequential formation of different layers of dystrophic neurites in Alzheimer's brains. *Mol Psychiatry* [Internet]. 2019 Sep 21;24(9):1369–82. Available from: [<URL>](#).
6. Rajmohan R, Reddy PH. Amyloid-Beta and Phosphorylated Tau Accumulations Cause Abnormalities at Synapses of Alzheimer's disease Neurons. *J Alzheimer's Dis* [Internet]. 2017 Apr 19;57(4):975–99. Available from: [<URL>](#).
7. Šimić G, Babić Leko M, Wray S, Harrington C, Delalle I, Jovanov-Milošević N, et al. Tau Protein Hyperphosphorylation and Aggregation in Alzheimer's Disease and Other Tauopathies, and Possible Neuroprotective Strategies. *Biomolecules* [Internet]. 2016 Jan 6;6(1):6. Available from: [<URL>](#).
8. Ben Zablah Y, Zhang H, Gugustea R, Jia Z. LIM-Kinases in Synaptic Plasticity, Memory, and Brain Diseases. *Cells* [Internet]. 2021 Aug 13;10(8):2079. Available from: [<URL>](#).
9. Manetti F. LIM kinases are attractive targets with many macromolecular partners and only a few small molecule regulators. *Med Res Rev* [Internet]. 2012 Sep 16;32(5):968–98. Available from: [<URL>](#).
10. Scott RW, Olson MF. LIM kinases: function, regulation and association with human disease. *J Mol Med* [Internet]. 2007 Jun 10;85(6):555–68. Available from: [<URL>](#).
11. Turab Naqvi AA, Hasan GM, Hassan MI. Targeting Tau Hyperphosphorylation via Kinase Inhibition: Strategy to Address Alzheimer's Disease. *Curr Top Med Chem* [Internet]. 2020 Jun 1;20(12):1059–73. Available from: [<URL>](#).
12. Hiraoka J, Okano I, Higuchi O, Yang N, Mizuno K. Self-association of LIM-kinase 1 mediated by the interaction between an N-terminal LIM domain and a C-terminal kinase domain. *FEBS Lett* [Internet]. 1996 Dec 9;399(1–2):117–21. Available from: [<URL>](#).
13. Park J, Kim SW, Cho MC. The Role of LIM Kinase in the Male Urogenital System. *Cells* [Internet]. 2021 Dec 28;11(1):78. Available from: [<URL>](#).
14. Ding Y, Milosavljevic T, Alahari SK. Nischarin Inhibits LIM Kinase To Regulate Cofilin Phosphorylation and Cell Invasion. *Mol Cell Biol* [Internet]. 2008 Jun 1;28(11):3742–56. Available from: [<URL>](#).
15. Bernard O. Lim kinases, regulators of actin dynamics. *Int J Biochem Cell Biol* [Internet]. 2007 Jan 1;39(6):1071–6. Available from: [<URL>](#).
16. Ohashi K. Roles of cofilin in development and its mechanisms of regulation. *Dev Growth Differ* [Internet]. 2015 May 10;57(4):275–90. Available from: [<URL>](#).

17. Henderson BW, Greathouse KM, Ramdas R, Walker CK, Rao TC, Bach S V., et al. Pharmacologic inhibition of LIMK1 provides dendritic spine resilience against β -amyloid. *Sci Signal* [Internet]. 2019 Jun 25;12(587):eaaw9318. Available from: [<URL>](#).
18. Singh R, Pokle AV, Ghosh P, Ganeshpurkar A, Swetha R, Singh SK, et al. Pharmacophore-based virtual screening, molecular docking and molecular dynamics simulations study for the identification of LIM kinase-1 inhibitors. *J Biomol Struct Dyn* [Internet]. 2023 Sep 2;41(13):6089–103. Available from: [<URL>](#).
19. Rangaswamy R, Hemavathy N, Subramaniyan S, Vetrivel U, Jeyakanthan J. Harnessing allosteric inhibition: prioritizing LIMK2 inhibitors for targeted cancer therapy through pharmacophore-based virtual screening and essential molecular dynamics. *J Biomol Struct Dyn* [Internet]. 2023 Dec 8; Article in Press. Available from: [<URL>](#).
20. Zhang M, Wang R, Tian J, Song M, Zhao R, Liu K, et al. Targeting LIMK1 with luteolin inhibits the growth of lung cancer in vitro and in vivo. *J Cell Mol Med* [Internet]. 2021 Jun 13;25(12):5560–71. Available from: [<URL>](#).
21. Daina A, Michielin O, Zoete V. SwissADME: a free web tool to evaluate pharmacokinetics, drug-likeness and medicinal chemistry friendliness of small molecules. *Sci Rep* [Internet]. 2017 Mar 3;7(1):42717. Available from: [<URL>](#).
22. Chen X, Li H, Tian L, Li Q, Luo J, Zhang Y. Analysis of the Physicochemical Properties of Acaricides Based on Lipinski's Rule of Five. *J Comput Biol* [Internet]. 2020 Sep 1;27(9):1397–406. Available from: [<URL>](#).
23. Meihua Rose Feng BSP. Assessment of Blood-Brain Barrier Penetration: In Silico, In Vitro and In Vivo. *Curr Drug Metab* [Internet]. 2002 Dec 1;3(6):647–57. Available from: [<URL>](#).
24. Ejeh S, Uzairu A, Shallangwa GA, Abechi SE. In Silico Design, Drug-Likeness and ADMET Properties Estimation of Some Substituted Thienopyrimidines as HCV NS3/4A Protease Inhibitors. *Chem Africa* [Internet]. 2021 Sep 17;4(3):563–74. Available from: [<URL>](#).
25. Humphreys SC, Davis JA, Iqbal S, Kamel A, Kulmatycki K, Lao Y, et al. Considerations and recommendations for assessment of plasma protein binding and drug-drug interactions for siRNA therapeutics. *Nucleic Acids Res* [Internet]. 2022 Jun 24;50(11):6020–37. Available from: [<URL>](#).
26. Khan T, Dixit S, Ahmad R, Raza S, Azad I, Joshi S, et al. Molecular docking, PASS analysis, bioactivity score prediction, synthesis, characterization and biological activity evaluation of a functionalized 2-butanone thiosemicarbazone ligand and its complexes. *J Chem Biol* [Internet]. 2017 Jul 4;10(3):91–104. Available from: [<URL>](#).
27. Tariq M, Sirajuddin M, Ali S, Khalid N, Tahir MN, Khan H, et al. Pharmacological investigations and Petra/Osiris/Molinspiration (POM) analyses of newly synthesized potentially bioactive organotin(IV) carboxylates. *J Photochem Photobiol B Biol* [Internet]. 2016 May 1;158:174–83. Available from: [<URL>](#).
28. Abraham MJ, Murtola T, Schulz R, Páll S, Smith JC, Hess B, et al. GROMACS: High performance molecular simulations through multi-level parallelism from laptops to supercomputers. *SoftwareX* [Internet]. 2015 Sep 1;1–2:19–25. Available from: [<URL>](#).
29. Rakhshani H, Dehghanian E, Rahati A. Enhanced GROMACS: toward a better numerical simulation framework. *J Mol Model* [Internet]. 2019 Dec 25;25(12):355. Available from: [<URL>](#).
30. Parra-Cruz R, Jäger CM, Lau PL, Gomes RL, Pordea A. Rational Design of Thermostable Carbonic Anhydrase Mutants Using Molecular Dynamics Simulations. *J Phys Chem B* [Internet]. 2018 Sep 13;122(36):8526–36. Available from: [<URL>](#).
31. Das NC, Labala RK, Patra R, Chattoraj A, Mukherjee S. In Silico Identification of New Anti-SARS-CoV-2 Agents from Bioactive Phytocompounds Targeting the Viral Spike Glycoprotein and Human TLR4. *Lett Drug Des Discov* [Internet]. 2022 Mar 7;19(3):175–91. Available from: [<URL>](#).
32. Liu P, Lu J, Yu H, Ren N, Lockwood FE, Wang QJ. Lubricant shear thinning behavior correlated with variation of radius of gyration via molecular dynamics simulations. *J Chem Phys* [Internet]. 2017 Aug 28;147(8):84904. Available from: [<URL>](#).
33. Singh VK, Chaurasia H, Kumari P, Som A, Mishra R, Srivastava R, et al. Design, synthesis, and molecular dynamics simulation studies of quinoline derivatives as protease inhibitors against SARS-CoV-2. *J Biomol Struct Dyn* [Internet]. 2022 Dec 5;40(21):10519–42. Available from: [<URL>](#).